

# 3D Hand Pose Estimation in the Wild via Graph Refinement under Adversarial Learning

Yiming He\*, Wei Hu\*, Siyuan Yang<sup>†</sup>, Xiaochao Qu<sup>†</sup>, Pengfei Wan<sup>†</sup> and Zongming Guo\*

\*Peking University, <sup>†</sup>MtLab, Meitu Inc.

{hymeecs forhuwei guozongming}@pku.edu.cn

{ysy2 qxc wpf}@meitu.com

**Abstract**—This paper addresses the problem of 3D hand pose estimation from a monocular RGB image. While previous methods have shown their success, the structure of hands has not been exploited explicitly, which is critical in pose estimation. To this end, we propose a hand-model regularized graph refinement paradigm under an adversarial learning framework, aiming to explicitly capture structural inter-dependencies of hand joints for the learning of intrinsic patterns. We estimate an initial hand pose from a parametric hand model as a prior of hand structure, and refine the structure by learning the deformation of the prior pose via residual graph convolution. To optimize the hand structure further, we propose two bone-constrained loss functions, which characterize the morphable structure of hand poses explicitly. Also, we introduce an adversarial learning framework with a multi-source discriminator to capture structural features, which imposes the constraints onto the distribution of generated 3D hand poses for anthropomorphically valid hand poses. Extensive experiments demonstrate that our model sets the new state-of-the-art in 3D hand pose estimation from a monocular image on standard benchmarks.

## I. INTRODUCTION

3D human hand pose estimation is a long-standing problem in computer vision, which is critical for various applications such as virtual reality and augmented reality [15; 30]. Previous works attempt to estimate hand pose from depth images [11; 41; 50; 10] or in multi-view setups [29; 48]. However, due to the diversity and complexity of hand shape, gesture, occlusion, *etc.*, it still remains a challenging problem despite years of studies [32; 45; 46; 14].

As RGB cameras are more widely accessible than depth sensors, recent works focus mostly on 3D hand pose estimation from a monocular RGB image and have shown their efficiency [12; 4; 3; 5; 51]. Nevertheless, the structure of hands has not been exploited explicitly in previous works, which is critical in pose estimation. Also, unlike bodies and faces that have obvious local characteristics (*e.g.*, eyes on a face), hands exhibit almost uniform appearance. Consequently, estimated hand poses from existing methods are sometimes distorted and unnatural.

To this end, we propose a *hand-model regularized graph refinement* network trained under a generative adversarial learning framework, which aims to explicitly exploit structural inter-dependencies between the hand joints. To model the relations among hand joints, we estimate an initial hand pose from a parametric hand model as a prior of hand structure (“prior pose”), which efficiently captures the characteristics of

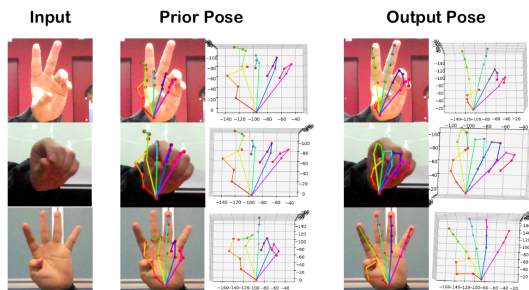


Fig. 1. The proposed method estimates 3D hand pose from a monocular image. Firstly a parametric hand model generates a *prior pose*, which serves as a structure prior and is then fed into a GCN refinement module for pose refinement under an adversarial learning framework, leading to state-of-the-art performance.

hand structures, *e.g.*, the adjacency relations between joints. Based on this prior pose, we represent the hand joints on a graph, where each joint is treated as a node and each pair of adjacent nodes are connected. We further learn the deformation of the prior pose to *refine* the hand structure by propagating information across adjacent nodes via residual graph convolution. Moreover, while most existing works [4; 12; 5] deploy 3D Euclidean distance between joints as the loss function for 3D annotation, we propose two bone loss functions that constrain the length and orientation of each bone connected by adjacent joints so as to preserve hand structure explicitly. On the other hand, to address the challenge of uniform appearance, we propose to train the network under an adversarial learning framework, aiming to estimate the real distribution of 3D hand poses. Besides, unlike recent works [12; 5; 19], we estimate 3D hand poses without resorting to ground truth meshes or depth maps, which is more suitable for datasets in the wild.

Specifically, given an input monocular image, our framework consists of a hand pose generator and a multi-source discriminator. The generator is composed of a modified MANO hand model [33] module that provides an initial pose estimation as prior pose and a Graph Convolutional Network (GCN) refinement module that refines the prior pose via residual graph convolution. In particular, taking the prior pose and image features as input, the GCN refinement module learns the deformation of the prior pose to refine the hand structure, by our designed residual graph convolution that leverages

on the recently proposed ResGCN [20]. Further, we design a multi-source discriminator that employs hand poses, hand bones computed from poses as well as the input image to distinguish the predicted 3D hand pose from the ground-truth, leading to anthropomorphically valid hand pose. The input poses and bones are fed into a GCN and a fully-connected layer respectively to learn intrinsic structural features of 3D hand pose, while the input image goes through a CNN to extract features of hand pose. These features are then concatenated and fed into a fully-connected layer to acquire the final decision. Experimental results demonstrate that our model achieves significant improvements over state-of-the-art approaches on standard benchmarks.

To summarize, our main contributions include

- We propose a hand-model regularized graph refinement network for 3D hand pose estimation from a monocular image, which explicitly exploits structural inter-dependencies between the hand joints. An initial pose estimation from a parametric hand model serves as the structure prior, which is then refined by learning the deformation via residual graph convolution.
- We introduce two bone-constrained loss functions, which optimize the estimation of hand structures by enforcing constraints on the topology of bones.
- We present an adversarial learning framework to impose structural constraints onto the distribution of generated 3D hand poses, which is able to address the challenge of uniform appearance in hands.
- Our method estimates 3D hand poses from a monocular image without resorting to additional sources such as ground truth meshes or depth maps, which is more suitable for datasets in the wild. Experimental results demonstrate that we set the new state-of-the-art.

## II. RELATED WORK

According to the input modalities, 3D hand pose estimation methods can be classified into three categories: 1) 3D hand pose estimation from depth images; 2) 3D hand pose estimation from multiple RGB images; 3) 3D hand pose estimation from a monocular RGB image.

### A. 3D hand pose estimation from depth images

Depth images contain rich 3D information [38] for hand pose estimation, which has shown promising accuracy [47]. There is a rich literature on 3D hand pose estimation with depth images as input [10; 11; 9; 7; 8; 17; 42; 22; 26]. Among them, some works [8; 17] are based on a deformable hand model with an iterative optimization training approach. A recent work [22] leverages CNN to learn the shape and pose parameters for a proposed model (LBS hand model).

### B. 3D hand pose estimation from multiple images

Multiple RGB images taken from different views also contain rich 3D information. Therefore, some works take multiple images as input [6; 28; 36] to alleviate the occlusion problem. Campos *et al.* [6] propose a regression-based approach for

hand pose estimation, where they utilize multi-view images to overcome the occlusion issue. Sridhar *et al.* [36] contribute a fundamentally extended generative tracking algorithm based on an augmented implicit shape representation with multiple images as input.

### C. 3D hand pose estimation from a monocular RGB image

Compared with the aforementioned two categories, a monocular RGB image is more accessible. Early works [2; 31; 37] propose complex model-fitting approaches, which are based on dynamics and multiple hypotheses and depend on restricted requirements. These model-fitting approaches have proposed many hand models, based on assembled geometric primitives [27] or sphere meshes [39], *etc.* Our work deploys the MANO hand model [33] as our prior, which models both hand shape and pose as well as generates meshes. Nevertheless, these sophisticated approaches suffer from low estimation accuracy.

With the advance of deep learning, many recent works estimate 3D hand pose from a monocular RGB image using neural networks [12; 4; 3; 5; 51; 43; 19]. Among them, some recent works [19; 12] directly reconstruct the 3D hand mesh and then generate the 3D hand pose through a pose regressor. [19] reconstructs the hand pose based on an auto-encoder, which employs an encoder to extract the latent code and feeds the latent code into the decoder to reconstruct hand mesh. Ge *et al.* [12] propose to estimate vertices of 3D meshes from GCNs [18] in order to learn nonlinear hand shape variations. The latent feature of the input RGB image is generated via several networks and then fed into a GCN to infer the 3D coordinates of mesh vertices. However, since the accuracy of the output hand mesh is critical for the two methods, both of them need extra dataset which provides ground truth hand mesh as supervision. Also, the upsampling layer used in [12] to reconstruct the hand mesh will cause a nonuniform distribution of nodes in mesh, which influences the accuracy of hand pose. In contrast, we *refine* a prior pose estimated from a parametric hand model via residual graph convolution rather than reconstructing hand pose from latent features, where the prior pose provides reliable adjacency between hand joints and enables an elegant structural refinement via graph convolution. Besides, our method does not require any additional supervision such as mesh supervision [12; 19] and depth image supervision [12; 5]. Hence, our method is more suitable for datasets in the wild. Further, we introduce adversarial training for 3D hand pose estimation, which enables learning a real distribution of 3D hand poses.

## III. METHODOLOGY

### A. Overview of the Proposed Approach

We aim to infer 3D hand pose via hand-model regularized graph refinement under an adversarial learning framework. The key is graph refinement of an initially estimated hand pose (*i.e.*, prior pose), which exploits the structural inter-dependencies among hand joints to correct fallacious topology

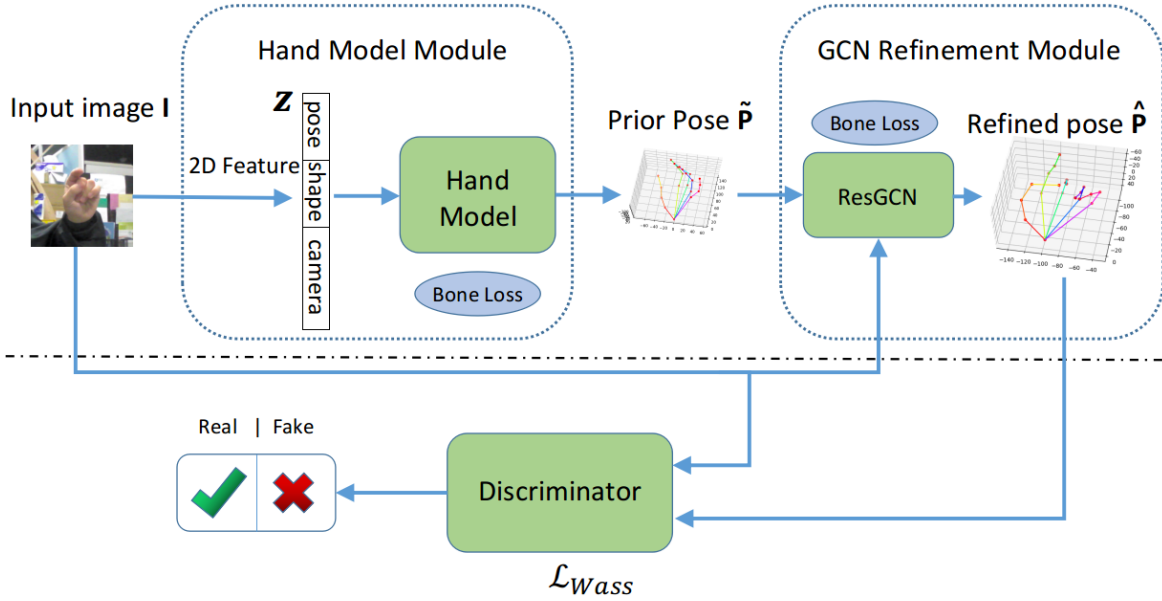


Fig. 2. Architecture of the proposed hand-model regularized graph refinement under an adversarial learning framework for 3D hand pose estimation.

in the prior pose. The entire framework consists of a generator  $\mathbb{G}$  and a discriminator  $\mathbb{D}$ , as illustrated in Fig. 2.

Given a monocular RGB image  $I$  as the input, the generator  $\mathbb{G}$  includes two modules:

- 1) The first module—*hand model module*—generates an initial estimation of 3D hand pose, which serves as a *prior pose* for the subsequent refinement. This module consists of a feature extractor and a parametric hand model. The feature extractor learns the latent code  $\mathbf{z}$  from the input image  $I$  as the parameters of the hand model. Subsequently, the hand model generates an initial 3D hand pose (prior pose)  $\tilde{\mathbf{P}}$  from the latent code.
- 2) The second module—*GCN refinement module*—aims at *pose refinement* of the prior pose  $\tilde{\mathbf{P}}$ . Taking  $\tilde{\mathbf{P}}$  and  $I$  as the input, the GCN refinement module explicitly exploits the structural relationship between adjacent hand joints via residual learning and outputs the deformation of the 3D hand pose, leading to the refined pose  $\hat{\mathbf{P}}$ .

The multi-source discriminator  $\mathbb{D}$  imposes structural constraints onto the distribution of generated 3D hand poses, which distinguishes the ground-truth 3D poses from the predicted ones. In particular, we explicitly incorporate structural properties of hand pose and bones into the discriminator, by employing three input sources: 1) the 3D hand pose  $\hat{\mathbf{P}}$ ; 2) the hand bone matrix, which is inferred from the 3D hand pose; and 3) the original image  $I$ . This enables learning the intrinsic structure of hand poses.

### B. The Proposed Generator $\mathbb{G}$

To exploit structural relationship between hand joints, we take advantage of existing parametric hand models to generate an initial estimation of hand pose as prior pose and then refine

the prior pose via residual graph convolution. We discuss the two modules of the generator in detail as follows.

1) *The hand model module:* Given an input monocular image, this module aims to generate an initial estimation of 3D hand pose  $\tilde{\mathbf{P}}$ , which serves as a prior pose for the subsequent hand pose refinement. A hand model is able to represent both hand shape and pose with a few parameters, which is thus a suitable prior for hand pose estimation.

We first predict parameters of the hand model. Specifically, we crop and resize the input image to a saliency region of the hand, which is fed into the ResNet-50 [13] to extract features for the construction of the latent code  $\mathbf{z}$ , *i.e.*, parameters of the hand model. Then, we employ a modified MANO hand model [33], which is based on the SMPL model [21] for human bodies. The MANO hand model is a deformable hand mesh model with two vectors  $\theta$  and  $\beta$  contained in the latent code  $\mathbf{z}$  as the input, which control the pose and shape of the generated hand respectively. The output of the MANO hand model includes a hand pose  $\mathcal{P}(\theta, \beta)$ .

Additionally, we need to position the pose  $\mathcal{P}(\theta, \beta)$  in a camera coordinate system so as to acquire the 3D coordinates of each point in the hand pose. We project  $\mathcal{P}(\theta, \beta)$  to the 3D space via three parameters that model the camera coordinate system: 1) a 3D rotation parameter  $\mathbf{c}_r \in \mathbb{R}^3$ ; 2) a 3D translation parameter  $\mathbf{c}_t \in \mathbb{R}^3$ ; and 3) a scale parameter  $\mathbf{c}_s \in \mathbb{R}$ . We formulate the complete hand model as:

$$\tilde{\mathbf{P}}(\theta, \beta, \mathbf{c}_r, \mathbf{c}_t, \mathbf{c}_s) = \mathbf{c}_s * R(\mathcal{P}(\theta, \beta), \mathbf{c}_r) + \mathbf{c}_t, \quad (1)$$

where  $R$  is a rotation function. The acquired initial estimation  $\tilde{\mathbf{P}}$  serves as a prior pose for the subsequent GCN refinement model.

2) *The GCN Refinement Module:* The GCN refinement module aims to refine the intrinsic structure of the prior pose

$\tilde{\mathbf{P}}$ . Since keypoints in 3D hand pose  $\tilde{\mathbf{P}}$  reside on irregular grids, it is natural to represent them on a graph and employ graph convolution for pose refinement.

Instead of directly generating a new hand pose, we take the initial estimation  $\tilde{\mathbf{P}}$  as a prior, and learn the *deformation* of  $\tilde{\mathbf{P}}$  with the supervision of the ground truth hand pose. Further, since the input RGB image  $\mathbf{I}$  contains prominent information about the hand pose, we exploit the connection between image cues and 3D poses to alleviate the ambiguity of 3D human pose estimation. Formally, the refined pose is

$$\hat{\mathbf{P}} = \tilde{\mathbf{P}} + \text{GCN}(\tilde{\mathbf{P}} \oplus \mathbf{f}), \quad (2)$$

where  $\mathbf{f}$  denotes the feature vector of the 2D image and  $\oplus$  denotes the concatenation operation.  $\text{GCN}(\tilde{\mathbf{P}} \oplus \mathbf{f})$  represents the learned deformation between the prior  $\tilde{\mathbf{P}}$  and the ground truth. The sum of the prior pose  $\tilde{\mathbf{P}}$  and its deformation thus leads to the refined hand pose.

Specifically, we first extract features from the RGB image  $\mathbf{I}$  to facilitate the pose refinement. We follow the ResNet-50 architecture [13] to extract 2D features  $\mathbf{f}$  from  $\mathbf{I}$ . Then, we represent the prior pose on an unweighted graph, where we treat each keypoint (*i.e.*, joint) on the hand as a node in the graph and connect nodes according to the human hand structure. That is, adjacent joints belonging to the same finger are connected to each other, as demonstrated in the green part of Fig. 5.

Next, we refine the hand pose via residual graph convolution. Leveraging on the idea of the recent ResGCN [20] that shows graph residual learning enables deeper graph convolution networks and better feature learning, we design a *Graph Res-block* to learn the deformation of the prior pose. Specifically, we employ the efficient GCN [18] as the basic unit of the Graph Res-block, which essentially propagates information across adjacent nodes to learn higher-level features. Each Graph Res-block consists of two GCN layers as well as two normalization layers that enable higher learning rate without vanishing or exploding gradients. Furthermore, we introduce residual skip connections for all the Graph Res-blocks in order to accelerate the speed of convergence and avoid the gradient vanishment.

Let  $\mathbf{X}^l$  denote the input of the  $l$ th Graph Res-block, then the output of the  $l$ th Graph Res-block takes the form

$$\mathbf{X}^{l+1} = N(g(N(g(\mathbf{X}^l))) + \text{skip}(\mathbf{X}^l), \quad (3)$$

where  $g(\cdot)$  represents a single GCN layer as in [18],  $N(\cdot)$  represents a single normalization layer, and  $\text{skip}(\cdot)$  denotes the skip connection which is a single GCN layer. We then stack several layers of Graph Res-blocks to learn the deformation of the prior pose, as demonstrated in Fig. 3.

### C. The Proposed Discriminator $\mathbb{D}$

In the adversarial training stage, while we learn the generator to predict hand poses which are indistinguishable to the discriminator, the discriminator attempts to distinguish real samples from fake ones, *i.e.*, the predicted hand poses.

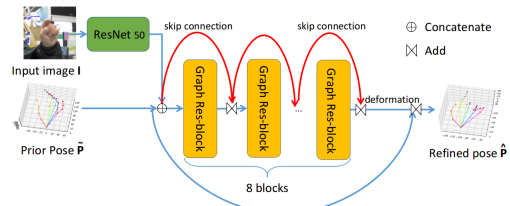


Fig. 3. Architecture of the GCN refinement module in our generator.

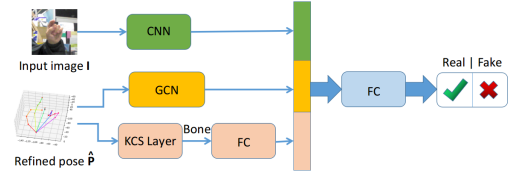


Fig. 4. Architecture of the multi-source discriminator. The discriminator includes features of three sources: 1) the original image; 2) the refined hand pose; 3) the hand bone matrix computed from the refined hand pose.

A simple architecture of a discriminator is a fully-connected (FC) network with the hand pose as input, which however has two shortcomings: 1) the relation between the RGB image and refined hand pose is neglected; 2) structural properties of the hand pose are not taken into account explicitly. Instead, inspired by the multi-source architecture in [44], we design a multi-source discriminator with three inputs to address the aforementioned issues. As illustrated in Fig. 4, the inputs include: 1) features of the input monocular image; 2) features of the refined hand pose  $\hat{\mathbf{P}}$ ; 3) features of bones computed from the refined hand pose  $\hat{\mathbf{P}}$  via the KCS layer as in [40], which computes the bone matrix from  $\hat{\mathbf{P}}$  via a simple matrix multiplication. The bone features contain prominent structural information such as the length and direction of bones, thus characterizing the hand structure accurately.

Specifically, we employ a CNN to extract the features of the input monocular image, a GCN to learn the representation of the refined hand pose and one fully-connected layer to capture the features of bone structures computed from the refined hand pose. Besides, the architecture of our multi-source discriminator is based on SNGAN [23] with spectral normalization layers. We take the Wasserstein loss function in [1] as the loss of our discriminator.

### D. The Proposed Bone-Constrained Loss Functions

The loss functions in previous hand pose estimation methods measure the average distance in the coordinates of joints of 3D hand pose and that of projected 2D hand pose [4; 12; 5], which we refer to as  $\mathcal{L}_{\text{pose}}$  and  $\mathcal{L}_{\text{proj}}$  respectively. However, these two loss functions cannot capture the structural properties of hand pose efficiently. Hence, we propose two novel bone-constrained loss functions to characterize the length and direction of each bone.

As illustrated in Fig. 5, we first define a bone vector  $\mathbf{b}_{i,j}$

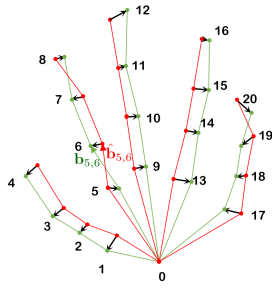


Fig. 5. Illustration of the residual between the ground truth hand pose (marked in green) and the predicted one (marked in red). Each hand pose has 21 key joints. We denote a bone vector connecting two key joints  $i$  and  $j$  by  $\mathbf{b}_{i,j}$ , such as  $\mathbf{b}_{5,6}$  in the figure.

between hand joint  $i$  and  $j$  as

$$\mathbf{b}_{i,j} = \mathbf{j}_i - \mathbf{j}_j, \quad (4)$$

where  $\mathbf{j}_i, \mathbf{j}_j \in \mathbb{R}^{3 \times 1}$  are the coordinates of joint  $i$  and  $j$  respectively.

The first bone-constrained loss  $\mathcal{L}_{\text{len}}$  quantifies the distance in *bone length* between the ground truth hand and its estimate, which we define as

$$\mathcal{L}_{\text{len}} = \sum_{i,j} \left| \|\mathbf{b}_{i,j}\|_2 - \|\hat{\mathbf{b}}_{i,j}\|_2 \right|, \quad (5)$$

where  $\mathbf{b}_{i,j}$  and  $\hat{\mathbf{b}}_{i,j}$  are the bone vectors of the ground truth and the predicted bone respectively.

The second bone-constrained loss  $\mathcal{L}_{\text{dir}}$  measures the deviation in the *direction of bones*:

$$\mathcal{L}_{\text{dir}} = \sum_{i,j} \left\| \left\| \mathbf{b}_{i,j} / \|\mathbf{b}_{i,j}\|_2 - \hat{\mathbf{b}}_{i,j} / \|\hat{\mathbf{b}}_{i,j}\|_2 \right\|_2 \right\|_2. \quad (6)$$

This is motivated by the fact that small loss in joints sometimes may not reflect large distortion in hand pose. Taking joints  $\mathbf{j}_5$  and  $\mathbf{j}_6$  in Fig. 5 as an example, the distance between the ground truth joints and predicted ones is trivial. However, it is obvious that the orientation of the predicted bone  $\hat{\mathbf{b}}_{5,6}$  significantly deviates from the ground truth  $\mathbf{b}_{5,6}$ . This distortion in hand structure is well captured by our proposed loss in bone direction  $\mathcal{L}_{\text{dir}}$ .

Besides, as we adopt the framework of adversarial learning, we also introduce the Wasserstein loss  $\mathcal{L}_{\text{Wass}}$  into the loss function for adversarial training. Hence, the overall loss function  $\mathcal{L}$  is

$$\mathcal{L} = \mathcal{L}_{\text{pose}} + \lambda_{\text{proj}} \mathcal{L}_{\text{proj}} + \lambda_{\text{len}} \mathcal{L}_{\text{len}} + \lambda_{\text{dir}} \mathcal{L}_{\text{dir}} + \lambda_{\text{Wass}} \mathcal{L}_{\text{Wass}}, \quad (7)$$

where  $\lambda_{\text{proj}}$ ,  $\lambda_{\text{len}}$ ,  $\lambda_{\text{dir}}$  and  $\lambda_{\text{Wass}}$  are hyperparameters for the trade-off among these losses.

## IV. EXPERIMENTAL RESULTS

### A. Datasets and Metrics

**Datasets** We evaluate our approach on two publicly available datasets: Stereo Hand Pose Tracking Benchmark (STB) [49] and the Rendered Hand Pose Dataset (RHD) [52].

| Stage | hand model | refinement | discriminator | STB           | RHD            |
|-------|------------|------------|---------------|---------------|----------------|
| I     | ✓          |            |               | 24.1534       | 83.3669        |
| II    | ✓          | ✓          |               | 5.1153        | 15.8356        |
| III   | ✓          | ✓          | ✓             | <b>3.9664</b> | <b>12.4036</b> |

TABLE I  
THE PERFORMANCE OF DIFFERENT STAGES IN OUR MODEL ON THE STB AND RHD DATASETS (MEASURED IN 3D EUCLIDEAN DISTANCE (MM)).

| Model | GCN refinement | FC refinement | discriminator | STB           | RHD            |
|-------|----------------|---------------|---------------|---------------|----------------|
| 1     |                | ✓             |               | 15.1134       | 37.5908        |
| 2     | ✓              |               |               | 5.1153        | 15.8356        |
| 3     |                | ✓             | ✓             | 10.2345       | 25.1456        |
| 4     | ✓              |               | ✓             | <b>3.9664</b> | <b>12.4036</b> |

TABLE II  
ABLATION STUDIES ON THE REFINEMENT MODULE. COMPARISON BETWEEN THE GCN REFINEMENT MODULE AND THE SIMPLE FC REFINEMENT MODULE IN 3D EUCLIDEAN DISTANCE (MM).

STB is a real-world dataset with image resolution of  $640 \times 320$ . STB contains two subsets: one subset is captured by a Point Grey Bumblebee2 stereo camera (STB-BB) and the other is captured by an active depth camera (STB-SK). Following the setting in previous works [5], we only use the STB-SK subset which contains 18,000 images with the ground truth of 21 hand joint locations. Following [52], we split the 18,000 images into 15,000 training samples and 3,000 test samples. During the training, we crop and resize the images into  $224 \times 224$ . Besides, to make the definition of joints consistent, we move the location of the root joint from the palm center to the wrist following [12].

RHD is a more challenging synthetic dataset with image resolution of  $320 \times 320$ , which is built upon 20 different characters performing 39 actions. It consists of 41,258 images for training and 2,728 images for testing. All samples are annotated with the location of 2D and 3D key points. Compared to STB, RHD is more challenging due to the large variations in viewpoints. We also crop and resize the images into  $224 \times 224$  during the training.

**Metrics** We evaluate the performance of 3D hand pose estimation with two metrics: (i) pose error, which takes the average location error in Euclidean distance between the estimated 3D joints and the ground truth; (ii) percentage of correct key points (PCK), which is the percentage of correct key points whose error in Euclidean distance is below a threshold.

### B. Implementation Details

In our experiments, we first pretrain the hand model module and then train the entire network end-to-end. In particular, the training process can be divided into three stages.

**Stage I.** In the first stage, we pretrain the hand model module, which is randomly initialized and trained for 100 epochs using the Adam optimizer with learning rate 0.001.

**Stage II.** In the second stage, we train the generator  $\mathbb{G}$  end-to-end without the discriminator  $\mathbb{D}$ . In  $\mathbb{G}$ , the hand model module is initialized with the trained model in the first stage

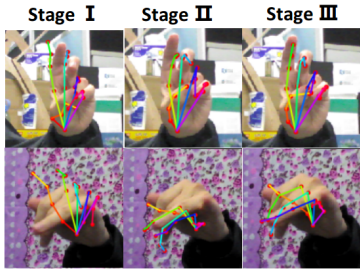


Fig. 6. Qualitative results of different stages in our model.

and the GCN refinement module is randomly initialized.  $\mathbb{G}$  is then trained with 100 epochs using the Adam optimizer with learning rate 0.0001. The finally predicted hand pose is much finer than that of stage I after training the entire generator.

**Stage III.** In the third stage, we adopt the framework of SNGAN [23] for the adversarial training and train our model end-to-end.  $\mathbb{G}$  and  $\mathbb{D}$  is trained with 100 epochs using the Adam optimizer with learning rate 0.0001.

For the hyperparameters in (7), we set  $\lambda_{\text{len}} = 0.01$ ,  $\lambda_{\text{dir}} = 0.1$ ,  $\lambda_{\text{proj}} = 0.1$ ,  $\lambda_{\text{Wass}} = 0.01$  in our implementation.

### C. Ablation Studies

We perform ablation studies on the performance of different stages, the graph refinement module, the discriminator and loss functions. We present all the results in 3D Euclidean distance (mm). Please refer to the supplementary material for the results measured in 3D PCK.

**On different stages.** We present the results of three training stages in average 3D Euclidean distance, as listed in in Tab. I. The performance of **Stage II** significantly outperform **Stage I**, which demonstrates that the proposed GCN refinement module plays the most critical role in our model. The adversarial training scheme (**Stage III**) further improves the result, by learning a real distribution of the 3D hand pose. We also show visual results of our method at different stages in Fig. 6. We see that Stage I estimates a coarse hand pose from the MANO hand model as a prior pose, while Stage II refines the structure of the prior pose significantly. Finally, Stage III generates more realistic hand poses via adversarial learning.

**On the GCN refinement module.** To evaluate the performance improvement achieved by the GCN refinement module, we compare the GCN refinement module with a simple fully-connected refinement module (FC Refinement Module) to refine the prior pose. We train the refinement modules in different experimental settings: 1) without our discriminator, *i.e.*, without adversarial learning; and 2) with our discriminator. As presented in Tab. II, the GCN refinement module leads to significant gain over the simple FC refinement module on both datasets in different settings, thus validating the superiority of the proposed GCN refinement module.

**On the discriminator.** To evaluate the importance of the proposed multi-source discriminator, we compare with a single-source discriminator which only takes the 3D hand pose

| Model | refinement | multi-source | single-source | STB           | RHD            |
|-------|------------|--------------|---------------|---------------|----------------|
| 1     | ✓          | ✓            |               | <b>3.9664</b> | <b>12.4036</b> |
| 2     | ✓          |              | ✓             | 4.5397        | 15.0987        |

TABLE III  
ABLATION STUDIES ON THE DISCRIMINATOR (3D EUCLIDEAN DISTANCE (MM)).

| Model | $\mathcal{L}_{\text{pose}} + \mathcal{L}_{\text{proj}}$ | $\mathcal{L}_{\text{len}}$ | $\mathcal{L}_{\text{dir}}$ | STB     |          |               | RHD     |          |                |
|-------|---|----------------------------|----------------------------|---------|----------|---------------|---------|----------|----------------|
|       |   |                            |                            | Stage I | Stage II | Stage III     | Stage I | Stage II | Stage III      |
| 1     | ✓   |                            |                            | 32.7531 | 9.1134   | 5.3456        | 99.2375 | 25.9614  | 15.0731        |
| 2     | ✓   | ✓                          |                            | 30.3156 | 8.0021   | 5.0175        | 95.1854 | 22.9613  | 14.7620        |
| 3     | ✓   |                            | ✓                          | 27.6512 | 6.9146   | 4.9980        | 89.7623 | 21.6328  | 14.0072        |
| 4     | ✓   | ✓                          | ✓                          | 24.1534 | 5.1153   | <b>3.9664</b> | 83.3669 | 15.8356  | <b>12.4036</b> |

TABLE IV  
ABLATION STUDIES ON THE PROPOSED BONE-CONSTRAINED LOSS FUNCTIONS AT THREE STAGES.

as the input. As presented in Tab. III, our multi-source discriminator outperforms the single-source one on both datasets, which gives credits to exploring the structure of hand bones and the relation between the image and hand pose.

**On loss functions.** We also evaluate the proposed bone-constrained loss functions  $\mathcal{L}_{\text{len}}$  and  $\mathcal{L}_{\text{dir}}$  separately. We train the network with different combinations of loss functions on the STB and RHD datasets in three stages respectively. As reported in Tab. IV, the network trained with our proposed bone-constrained loss functions performs better in all the three stages on both datasets. We also notice that the bone direction loss  $\mathcal{L}_{\text{dir}}$  plays a more significant role compared to  $\mathcal{L}_{\text{len}}$ . This gives credits to the constraint on the orientation of bones that explicitly takes structural properties of human hands into consideration. Further, we demonstrate the visual comparison of estimated poses with and without bone-constrained losses in Fig. 7. We observe that the estimated pose may have unnatural distortion in the direction of bones in the absence of the bone-constrained loss functions, *e.g.*, the little finger in the first row and the thumb in the second row. In contrast, our results exhibit natural and accurate structure in the orientation of bones with the proposed bone constraints enforced.

### D. Experimental Results

We compare our method with competitive 3D hand pose estimation approaches on the RHD and STB datasets. On the relatively simple STB dataset, as shown in Fig. 8(a)(b), we compare with latest methods [5; 16; 4; 12; 24; 51; 25]. Our paradigm outperforms the state-of-the-art [12], which closely reaches the upper bound 1.0 of 3D PCK at all the error thresholds. Moreover, since it is a bit difficult to distinguish our method with the state-of-the-art in Fig. 8(a), we provide sole comparison with the state-of-the-art in Fig. 8(b). Also, we list the results in 3D Euclidean distance for comparison with the state-of-the-arts in Tab. V. Compared to these works which directly reconstruct the 3D hand pose [12; 4; 5], our method performs much better mainly due to the proposed GCN refinement module and the adversarial training approach.

On the more challenging RHD dataset, we compare with latest competitive approaches [12; 5; 35; 51]. As presented in

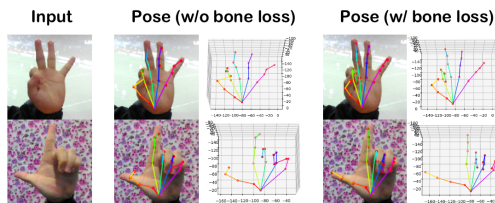


Fig. 7. Qualitative results for the evaluation of the proposed bone-constrained loss functions.

|                       | Ours     |           | Ge et al. [12] | Boukhayma et al. [4] | Cai et al. [5] |
|-----------------------|----------|-----------|----------------|----------------------|----------------|
|                       | Stage II | Stage III |                |                      |                |
| 3D Euclidean distance | 5.12     | 3.97      | 6.37           | 9.76                 | 7.24           |

TABLE V

COMPARISON WITH STATE-OF-THE-ART METHODS ON THE STB DATASET (3D EUCLIDEAN DISTANCE (MM)).

Fig. 8(c), we significantly outperform the state-of-the-art [12] by 3% on average over all the error thresholds, thus validating the superiority of our method even on such a challenging dataset.

Moreover, we demonstrate some qualitative results of our 3D hand pose estimation in Fig. 9. The generated poses are accurate and natural even in case of severe self-occlusions, as shown in the first three columns of Fig. 9. This validates the effectiveness of the proposed paradigm. We show the qualitative results on the RHD dataset and a real-world dataset MPII+NZSL [34] in the supplementary material.

### E. Computation Complexity

While we set the new state-of-the-art on both datasets, the computational complexity is comparable to previous methods. When evaluated on one Nvidia GTX 1080ti GPU, the run-time of our full model is 25.1ms on average, including 15.3ms for the Hand Model Module and 9.8ms for the GCN Refinement Module. Hence, our method can run on GPU in real-time at about 40fps.

## V. CONCLUSION

In this paper, we propose a hand-model regularized graph refinement network under an adversarial learning framework, aiming to fully exploit the structural relations between hand joints. We take an initial estimation of hand pose as prior pose, and refine the prior pose by learning the deformation in structure via residual graph convolution. Also, we propose two bone-constrained loss functions to enforce constraints on the bone structures explicitly. Further, we present an adversarial learning framework to impose structural constraints onto the distribution of the generated 3D hand pose. Extensive experiments demonstrate that we significantly outperform state-of-the-art approaches, validating the superiority of the proposed method.

## REFERENCES

- [1] Martin Arjovsky, Soumith Chintala, and Léon Bottou. Wasserstein generative adversarial networks. In Doina Precup and Yee Whye Teh, editors, *Proceedings of the 34th International Conference on Machine Learning*, volume 70 of *Proceedings of Machine Learning Research*,

- pages 214–223, International Convention Centre, Sydney, Australia, 06–11 Aug 2017. PMLR.
- [2] Vassilis Athitsos and Stan Sclaroff. Estimating 3d hand pose from a cluttered image. In *IEEE Computer Society Conference on Computer Vision & Pattern Recognition*, 2003.
- [3] Seungryul Baek, Kwang In Kim, and Tae-Kyun Kim. Pushing the envelope for rgb-based dense 3d hand pose estimation via neural rendering. In *The IEEE Conference on Computer Vision and Pattern Recognition (CVPR)*, June 2019.
- [4] Adnane Boukhayma, Rodrigo de Bem, and Philip H.S. Torr. 3d hand shape and pose from images in the wild. In *The IEEE Conference on Computer Vision and Pattern Recognition (CVPR)*, June 2019.
- [5] Yujun Cai, Lihao Ge, Jianfei Cai, and Junsong Yuan. Weakly-supervised 3d hand pose estimation from monocular rgb images. In *The European Conference on Computer Vision (ECCV)*, September 2018.
- [6] T. E. De Campos and D. W. Murray. Regression-based hand pose estimation from multiple cameras. In *IEEE Computer Society Conference on Computer Vision & Pattern Recognition*, 2006.
- [7] Chiho Choi. Deephand: Robust hand pose estimation by completing a matrix imputed with deep features. In *Computer Vision & Pattern Recognition*, 2016.
- [8] La Gorce M De, D. J. Fleet, and N Paragios. Model-based 3d hand pose estimation from monocular video. *IEEE Trans Pattern Anal Mach Intell*, 33(9):1793–1805, 2011.
- [9] Andrew Fitzgibbon. Accurate, robust, and flexible real-time hand tracking. *Proceedings*, pages 3633–3642, 2015.
- [10] Lihao Ge, Yujun Cai, Junwu Weng, and Junsong Yuan. Hand pointnet: 3d hand pose estimation using point sets. pages 8417–8426, 06 2018.
- [11] Lihao Ge, Hui Liang, Junsong Yuan, and Daniel Thalmann. Robust 3d hand pose estimation in single depth images: From single-view cnn to multi-view cnns. In *The IEEE Conference on Computer Vision and Pattern Recognition (CVPR)*, June 2016.
- [12] Lihao Ge, Zhou Ren, Yuncheng Li, Zehao Xue, Yingying Wang, Jianfei Cai, and Junsong Yuan. 3d hand shape and pose estimation from a single rgb image. In *The IEEE Conference on Computer Vision and Pattern Recognition (CVPR)*, June 2019.
- [13] Kaiming He, Xiangyu Zhang, Shaoqing Ren, and Jian Sun. Deep residual learning for image recognition. In *The IEEE Conference on Computer Vision and Pattern Recognition (CVPR)*, June 2016.
- [14] Liang Hui, Junsong Yuan, Jun Lee, Lihao Ge, and Daniel Thalmann. Hough forest with optimized leaves for global hand pose estimation with arbitrary postures. *IEEE Transactions on Cybernetics*, PP(99):1–15, 2017.
- [15] Wolfgang Hürst and Casper van Wezel. Gesture-based interaction via finger tracking for mobile augmented reality. *Multimedia Tools and Applications*, 62:233–258, 2011.
- [16] Umar Iqbal, Pavlo Molchanov, Thomas Breuel Juergen Gall, and Jan Kautz. Hand pose estimation via latent 2.5d heatmap regression. In *The European Conference on Computer Vision (ECCV)*, September 2018.
- [17] Sameh Khamis, Jonathan Taylor, Jamie Shotton, Cem Keskin, Shahram Izadi, and Andrew Fitzgibbon. Learning an efficient model of hand shape variation from depth images. In *IEEE Conference on Computer Vision & Pattern Recognition*, 2015.
- [18] Thomas N. Kipf and Max Welling. Semi-supervised classification with graph convolutional networks. In *International Conference on Learning Representations (ICLR)*, 2017.
- [19] Dominik Kulon, Haoyang Wang, Riza Alp Güler, Michael M. Bronstein, and Stefanos Zafeiriou. Single image 3d hand reconstruction with mesh convolutions. In *BMVC*, September 2019.
- [20] Guohao Li, Matthias Muller, Ali Thabet, and Bernard Ghanem. Deep-gcn: Can gcns go as deep as cnns? In *The IEEE International Conference on Computer Vision (ICCV)*, October 2019.
- [21] Matthew Loper, Naureen Mahmood, Javier Romero, Gerard Pons-Moll, and Michael J. Black. Smpl: A skinned multi-person linear model. *ACM Trans. Graph.*, 34(6):248:1–248:16, October 2015.
- [22] Jameel Malik, Ahmed Elhayek, Fabrizio Nunnari, Kiran Varanasi, and Didier Stricker. Deephps: End-to-end estimation of 3d hand pose and shape by learning from synthetic depth. In *2018 International Conference on 3D Vision (3DV)*, 2018.

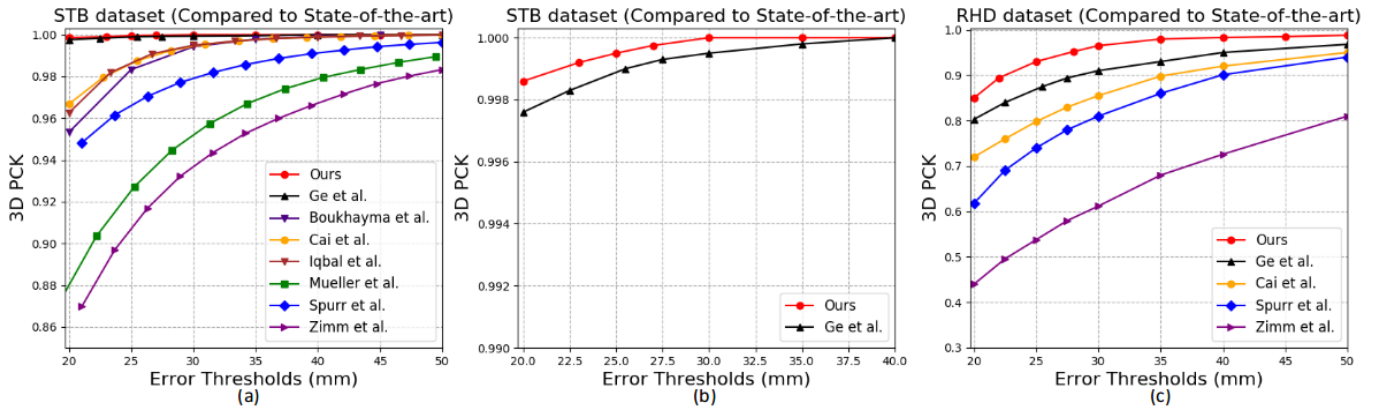


Fig. 8. Comparison with state-of-the-art methods on the STB and RHD datasets.

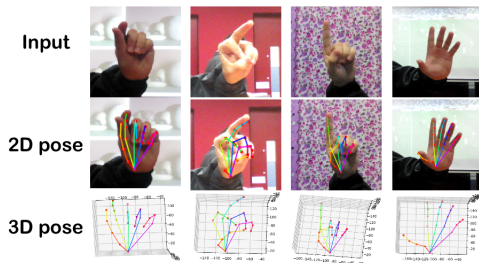


Fig. 9. Qualitative results of our proposed network on the STB dataset. The 2D pose is projected from the 3D pose.

- [23] Takeru Miyato, Toshiki Kataoka, Masanori Koyama, and Yuichi Yoshida. Spectral normalization for generative adversarial networks. In *International Conference on Learning Representations*, 2018.
- [24] Franziska Mueller, Florian Bernard, Oleksandr Sotnychenko, Dushyant Mehta, Srinath Sridhar, Dan Casas, and Christian Theobalt. Generated hands for real-time 3d hand tracking from monocular rgb. In *Proceedings of Computer Vision and Pattern Recognition (CVPR)*, June 2018.
- [25] Franziska Mueller, Florian Bernard, Oleksandr Sotnychenko, Dushyant Mehta, Srinath Sridhar, Dan Casas, and Christian Theobalt. Generated hands for real-time 3d hand tracking from monocular rgb. In *The IEEE Conference on Computer Vision and Pattern Recognition (CVPR)*, June 2018.
- [26] Markus Oberweger and Vincent Lepetit. Deepprior++: Improving fast and accurate 3d hand pose estimation. In *2017 IEEE International Conference on Computer Vision Workshops (ICCVW)*, 2018.
- [27] Iason Oikonomidis, Nikolaos Kyriazis, and Antonis Argyros. Efficient model-based 3d tracking of hand articulations using kinect. volume 1, 01 2011.
- [28] Iasonas Oikonomidis, Nikolaos Kyriazis, and Antonis A. Argyros. Markerless and efficient 26-dof hand pose recovery. In *Computer Vision-accv -asian Conference on Computer Vision*, 2010.
- [29] Paschalis Panteleris and Antonis A. Argyros. Back to RGB: 3d tracking of hands and hand-object interactions based on short-baseline stereo. *CoRR*, abs/1705.05301, 2017.
- [30] Thammathip Piumsomboon, Adrian Clark, Mark Billinghurst, and Andy Cockburn. User-defined gestures for augmented reality. In Paula Kotzé, Gary Marsden, Gitte Lindgaard, Janet Wesson, and Marco Winckler, editors, *Human-Computer Interaction – INTERACT 2013*, pages 282–299, Berlin, Heidelberg, 2013. Springer Berlin Heidelberg.
- [31] J. M. Rehg and T. Kanade. Digiteyes: vision-based hand tracking for human-computer interaction. In *IEEE Workshop on Motion of Non-rigid & Articulated Objects*, 2002.
- [32] James M. Rehg and Takeo Kanade. Visual tracking of high dof articulated structures: An application to human hand tracking. In *Proc of Third European Conference on Computer Vision*, 1994.
- [33] Javier Romero, Dimitrios Tzionas, and Michael J. Black. Embodied hands: Modeling and capturing hands and bodies together. *ACM Trans. Graph.*, 36(6):245:1–245:17, November 2017.
- [34] Tomas Simon, Hanbyul Joo, Iain Matthews, and Yaser Sheikh. Hand keypoint detection in single images using multiview bootstrapping. In *The IEEE Conference on Computer Vision and Pattern Recognition (CVPR)*, July 2017.
- [35] Adrian Spurr, Jie Song, Seonwook Park, and Otmar Hilliges. Cross-modal deep variational hand pose estimation. *CoRR*, abs/1803.11404, 2018.
- [36] S. Sridhar, H. Rhodin, H. P. Seidel, A. Oulasvirta, and C. Theobalt. Real-time hand tracking using a sum of anisotropic gaussians model. In *International Conference on 3D Vision*, 2014.
- [37] B. Stenger, A. Thayananthan, P. H. S. Torr, and R. Cipolla. Model-based hand tracking using a hierarchical bayesian filter. *IEEE Transactions on Pattern Analysis and Machine Intelligence*, 28(9):1372–1384, Sep. 2006.
- [38] Danhang Tang, Tsz Ho Yu, and Tae Kyun Kim. Real-time articulated hand pose estimation using semi-supervised transductive regression forests. In *IEEE International Conference on Computer Vision*, 2013.
- [39] Anastasia Tkach, Mark Pauly, and Andrea Tagliasacchi. Sphere-meshes for real-time hand modeling and tracking. *ACM Trans. Graph.*, 35(6):222:1–222:11, November 2016.
- [40] Bastian Wandt, Hanno Ackermann, and Bodo Rosenhahn. A kinematic chain space for monocular motion capture. 02 2017.
- [41] Xiaokun Wu, Daniel Finnegan, Eamonn O’Neill, and Yong-Liang Yang. Handmap: Robust hand pose estimation via intermediate dense guidance map supervision. In *The European Conference on Computer Vision (ECCV)*, September 2018.
- [42] Sun Xiao, Yichen Wei, Liang Shuang, Xiaou Tang, and Sun Jian. Cascaded hand pose regression. In *IEEE Conference on Computer Vision & Pattern Recognition*, 2015.
- [43] Linlin Yang and Angela Yao. Disentangling latent hands for image synthesis and pose estimation. In *The IEEE Conference on Computer Vision and Pattern Recognition (CVPR)*, June 2019.
- [44] Wei Yang, Wanli Ouyang, Xiaolong Wang, Jimmy Ren, Hongsheng Li, and Xiaogang Wang. 3d human pose estimation in the wild by adversarial learning. In *The IEEE Conference on Computer Vision and Pattern Recognition (CVPR)*, June 2018.
- [45] Wu Ying and T. S. Huang. Hand modeling, analysis and recognition. *IEEE Signal Processing Magazine*, 18(3):51–60, 2002.
- [46] Wu Ying, Lin John, and Thomas S Huang. Analyzing and capturing articulated hand motion in image sequences. *IEEE Transactions on Pattern Analysis & Machine Intelligence*, 27(12):1910–1922, 2005.



- [47] Shanxin Yuan, Guillermo Garcia-Hernando, Bjorn Stenger, Gyeongsik Moon, Ju Chang, Kyoung Lee, Pavlo Molchanov, Jan Kautz, Sina Honari, Liuhaio Ge, Junsong Yuan, Xinghao Chen, Guijin Wang, Fan Yang, Kai Akiyama, Yang Wu, Qingfu Wan, Meysam Madadi, Sergio Escalera, and Tae-Kyun Kim. Depth-based 3d hand pose estimation: From current achievements to future goals. pages 2636–2645, 06 2018.
- [48] Jiawei Zhang, Jianbo Jiao, Mingliang Chen, Liangqiong Qu, Xiaobin Xu, and Qingxiong Yang. 3d hand pose tracking and estimation using stereo matching. 10 2016.
- [49] Jiawei Zhang, Jianbo Jiao, Mingliang Chen, Liangqiong Qu, Xiaobin Xu, and Qingxiong Yang. 3d hand pose tracking and estimation using stereo matching. *ArXiv*, abs/1610.07214, 2016.
- [50] Yidan Zhou, Jian Lu, Kuo Du, Xiangbo Lin, Yi Sun, and Xiaohong Ma. Hbe: Hand branch ensemble network for real-time 3d hand pose estimation. In *The European Conference on Computer Vision (ECCV)*, September 2018.
- [51] Christian Zimmermann and Thomas Brox. Learning to estimate 3d hand pose from single rgb images. pages 4913–4921, 10 2017.
- [52] Christian Zimmermann and Thomas Brox. Learning to estimate 3d hand pose from single rgb images. In *The IEEE International Conference on Computer Vision (ICCV)*, Oct 2017.